Uniaxial Strain Control of Bulk Ferromagnetism in Rare-Earth Titanates

Najev, Ana; Hameed, S.; Gautreau, D.; Wang, Z.; Joe, J.; Požek, Miroslav; Birol, T.; Fernandes, R. M.; Greven, M.; Pelc, Damjan

Uniaxial Strain Control of Bulk Ferromagnetism in Rare-Earth Titanates

A. Najev,[1,2] S. Hameed,[2] D. Gautreau,[2,3] Z. Wang,[2] J. Joe,[2] M. Požek,[1] T. Birol,[3] R. M. Fernandes,[2] M. Greven,[2] and D. Pelc[1,2]

[1]*Department of Physics, Faculty of Science, University of Zagreb, Bijenička 32, HR-10000 Zagreb, Croatia*
[2]*School of Physics and Astronomy, University of Minnesota, Minneapolis, Minnesota 55455, USA*
[3]*Department of Chemical Engineering and Materials Science, University of Minnesota, Minneapolis, Minnesota 55455, USA*

(Received 13 May 2021; revised 26 October 2021; accepted 4 March 2022; published 20 April 2022)

The perovskite rare-earth titanates are model Mott insulators with magnetic ground states that are very sensitive to structural distortions. These distortions couple strongly to the orbital degrees of freedom and, in principle, it should be possible to tune the superexchange and the magnetic transition with strain. We investigate the representative system $(Y, La, Ca)TiO_3$, which exhibits low crystallographic symmetry and no structural instabilities. From magnetic susceptibility measurements of the Curie temperature, we demonstrate direct, reversible, and continuous control of ferromagnetism by influencing the TiO_6 octahedral tilts and rotations with uniaxial strain. The relative change in T_C as a function of strain is well described by *ab initio* calculations, which provides detailed understanding of the complex interactions among structural, orbital, and magnetic properties in rare-earth titanates. The demonstrated manipulation of octahedral distortions opens up far-reaching possibilities for investigations of electron-lattice coupling, competing ground states, and magnetic quantum phase transitions in a wide range of quantum materials.

DOI: 10.1103/PhysRevLett.128.167201

Transition-metal oxides exhibit a wealth of distinct structural, magnetic, and orbital ordering tendencies, and are thus among the most extensively studied condensed matter systems. A salient feature of these materials is the intricate interplay between structural and electronic properties: ferroelectric, metal-insulator, and superconducting transitions can all be strongly influenced by changes in the crystalline lattice. Importantly, the electronic ground states can thus be tuned by manipulating the structure. This has been employed in a wide range of materials, and led to significant breakthroughs, with the emergence of uniaxial strain as a particularly interesting control variable [1–11]. Prominent examples include the stabilization of ferroelectricity in epitaxially strained films of strontium titanate [1], as well as uniaxial stress manipulation of superconductivity in strontium ruthenate [5–7], metal-insulator transitions in vanadium oxides [8,9], superconductivity and charge-density-wave order in cuprates [2,10,12], and antiferromagnetism in pnictides [11]. However, this approach has so far relied either on the proximity to a structural instability or on the strain-induced lowering of structural symmetry, and it has not yet been applied to bulk ferromagnetic (FM) materials.

The trivalent rare-earth (RE) titanates $RTiO_3$ (R is a rare-earth ion) are prototypical three-dimensional Mott insulators [13] with rich phase diagrams [Fig. 1(a)] that are not fully understood. The R ion is surrounded by eight TiO_6 octahedra [14], but due to a considerable atomic-size mismatch, the lattice symmetry is orthorhombic (*Pbnm*), significantly lower than the ideal cubic perovskite. The TiO_6 octahedra are both tilted and rotated, and the distortions are more pronounced for smaller R ions, leading to larger deviations of the Ti—O—Ti bond angle from 180° [14] [Fig. 1(c)]. Since the orbital overlap strongly depends on the bond angles, so does the superexchange interaction between unpaired electron spins associated with the Ti $3d$ t_{2g} orbitals. Consequently, the spin-lattice coupling is strong [15–17], and the magnetism in RE titanates can be tuned by varying the average R-ion size: the magnetic ground state changes from FM to antiferromagnetic (AFM) with increasing R-ion size [18,19], or upon atomic substitution, e.g., in $Y_{1-x}La_xTiO_3$ (YLTO) [20,21] [Fig. 1(a)]. Charge doping can also be used to control the magnetic ground state, e.g., in $Y_{1-y}Ca_yTiO_3$ (YCTO), where hole doping destroys the long-range FM order at $y \sim 20\%$ and eventually leads to an insulator-metal transition [22,23]. Based on the behavior of thermal expansion coefficients across the magnetic transitions, it has been suggested that uniaxial strain might have an effect similar to atomic substitution; strain along the orthorhombic a direction should increase the octahedral distortions, stabilize the FM order, and increase the Curie temperature (T_C), whereas strain along b should decrease the distortion and T_C, similar to the substitution of Y with La [Fig. 1(c)] [15]. Attempts to control T_C with hydrostatic pressure were previously made for pressures up to 800 MPa [24]. However, the results show only a slight decrease of T_C.

In this Letter, we show that the Curie temperature of the YTO-based materials can be manipulated via *in situ* uniaxial stress in a remarkably wide range. We study both

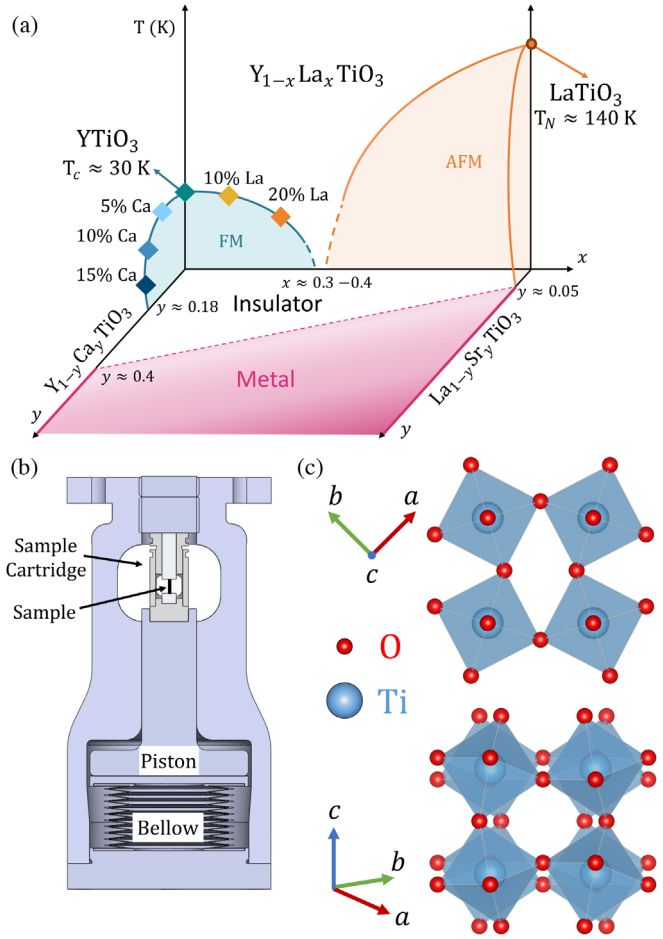

FIG. 1. (a) Phase diagram of $RTiO_3$ with FM (ferromagnetic), AFM (antiferromagnetic), insulating, and metallic phases. The compositions studied in this Letter are marked by diamonds. (b) Schematic of the uniaxial strain cell (for more details, see Ref. [25]). (c) $YTiO_3$ structure constructed from theory, showing the two relevant octahedral rotations, $a^0a^0c^+$ and $a^-a^-c^0$, as deviations from a simple cubic structure. Small spheres depict oxygen ions, large spheres titanium ions. Upper section: oxygen base plane with the $a^0a^0c^+$ rotation mode. Bottom section: perpendicular view showing the $a^-a^-c^0$ rotation mode. The effects of uniaxial stress along $a \equiv [100]$, $b \equiv [010]$, or $c \equiv [001]$ on the rotation modes are qualitatively different for each direction.

La- and Ca-substituted YTO, in the substitution range in which a FM ground state is observed [Fig. 1(a)], and demonstrate that T_C can be reversibly and continuously suppressed or enhanced by up to a factor of ~2, depending on the specific crystalline direction in which the uniaxial stress is applied. Moreover, we obtain nearly complete suppression of ferromagnetism in a Ca-substituted sample close to the FM-paramagnetic phase boundary. Through a comparison with *ab initio* and mean-field calculations, we show that the origin of the observed behavior is the strong effect of stress on the octahedral rotation distortions, and the pronounced sensitivity of the magnetic exchange couplings on these distortions. We thus demonstrate the potential of uniaxial stress engineering of oxygen octahedral rotations, which are present in most perovskite-based oxides, as a practical means to manipulate magnetism and induce quantum phase transitions.

We employ a uniaxial pressure-cell design [25] [Fig. 1(b)] that enables the application of high and spatially homogeneous uniaxial stress on millimeter-sized single crystals [32,33]. Force on the sample is generated with a helium pneumatic system, with bellows that expand when filled with pressurized gas and push on a piston that compresses the sample. By controlling the gas pressure, the force can be finely tuned. Samples are mounted within a cartridge with an inductive displacement sensor that allows independent determination of sample stress and strain. The strain-dependent magnetic susceptibility is measured *in situ* with either a mutual inductance setup or an inductance bridge [25]. The samples are single crystals of $YTiO_3$, YLTO, and YCTO, grown by the traveling-solvent floating-zone method [23,34,35], that were extensively characterized with Laue x-ray diffraction and polished to high precision along the orthorhombic directions a, b, and c.

The nonmagnetic symmetry of the RE titanate perovskites is low enough to preclude collinear magnetic order. As a result, spin canting is present in both FM and AFM phases, which have the same magnetic space group [17]. The FM moments in, e.g., $YTiO_3$, order predominantly along c, whereas the AFM moment in $LaTiO_3$ is predominantly of G type and orders along a [36]. No long-range structural changes are known to occur around the Curie and Néel temperatures, but due to the strong and anisotropic spin-lattice coupling, we observe significant effects of uniaxial stress on T_C. Representative ac susceptibility measurements for two samples, $Y_{0.9}Ca_{0.1}TiO_3$ and $Y_{0.85}Ca_{0.15}TiO_3$, are shown in Figs. 2(a) and 2(b), respectively. Both were deformed along b, which leads to a substantial decrease of T_C. The deformation is also seen to be reversible, despite the large stress values, as T_C before and after deformation is essentially the same. Moreover, the susceptibility curves and transition temperatures obtained for different stress levels are quite smooth, suggesting that no structural transitions occur with applied stress [25]. The Ca-15% sample is close to the boundary of FM order in the phase diagram of YCTO, and we were able to suppress the magnetism almost completely with strain. Interestingly, T_C appears to level off at high strain, but the magnitude of the susceptibility peak decreases toward zero. A possible explanation for this is that the FM volume fraction gradually decreases to zero with increasing uniaxial strain, thereby reducing the average bulk ordered moment. This would be indicative of a first-order rather than a second-order transition between the FM and paramagnetic phases, with the associated phase separation influenced by strain.

Figure 3 summarizes the Curie temperatures of all measured samples in a stress versus T_C phase diagram.

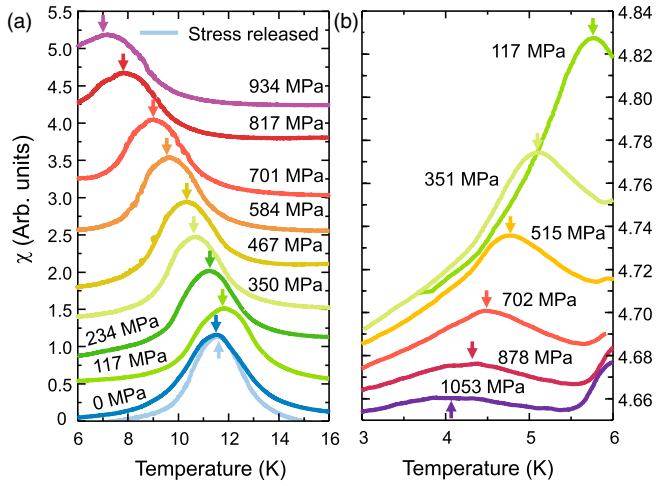

FIG. 2. Raw ac susceptibility data for (a) $Y_{0.9}Ca_{0.1}TiO_3$ and (b) $Y_{0.85}Ca_{0.15}TiO_3$, with applied stress along b and susceptibility measured along c. The Curie temperatures are taken as the peak positions (arrows). Data for different sample stresses are shifted vertically for clarity. In (a), the negligible increase of the susceptibility peak width with increasing stress indicates that the strain is homogeneously distributed in the sample; see Ref. [25] for the extracted full-width-at-half-maximum values. After stress release, T_C returns to its original value; the peak narrows slightly, indicative of residual inhomogeneous stress in the samples that decreases after the application of external pressure. In (b), the FM order disappears at a nonzero temperature, consistent with a first-order transition into a paramagnetic state. The small peak around 6 K likely originates from superconducting solder in the detection coils [25].

Our results directly confirm the proposed qualitative phase diagram of Ref. [15]: Stress along b and c decreases T_C, whereas compression along a promotes ferromagnetism and increases T_C. Our measurements reveal a sizable nonlinearity of T_C at high stress values and, as noted, a leveling off of T_C as the FM-paramagnetic phase boundary is approached with increasing stress in $Y_{0.85}Ca_{0.15}TO_3$. Although the influence of pressure on T_C qualitatively agrees with the predicted phase diagram, we note that significant irreversibility appears for stress along c, even at stress levels as low as 100 MPa, with T_C decreasing only slightly after an initial shift (see Ref. [25] for details). This effect is most prominent for the doped samples and might be related to intrinsic structural inhomogeneity. In contrast, when stress is applied along a and b, the strain (and therefore the change in T_C) is highly reversible.

With the exception of $Y_{0.85}Ca_{0.15}TO_4$, the dependence of T_C on stress is qualitatively similar for all studied samples. To perform a quantitative comparison, we introduce the scaling parameter σ_0, an effective elastic modulus that connects applied stress and octahedral distortions. We take the reference value $\sigma_0 = 1$ GPa for $YTiO_3$, and then adjust σ_0 for doped samples to obtain the scaling shown in Fig. 3(b) (see Ref. [25] for σ_0 values). All data for stress along b (except for Ca-15%, as noted) collapse on the master curve, with the doping-dependent σ_0 as the only free parameters. This suggests that neither Ca doping nor La doping fundamentally changes the physics of spin-lattice coupling, at least for doping levels not too close to the FM-paramagnetic boundary. Instead, doping mainly affects the mechanical properties: σ_0 increases with doping [25], implying that the lattice is more susceptible to tilts for a given applied stress.

In order to model the observed stress dependence of T_C and to elucidate the connection between the crystal structure and magnetic interactions, we performed first-principles density functional theory (DFT) calculations for $YTiO_3$ to predict the crystal structure and the exchange parameters for a Heisenberg model under uniaxial stress along each of the orthorhombic principal axes [25]. Calculations for doped

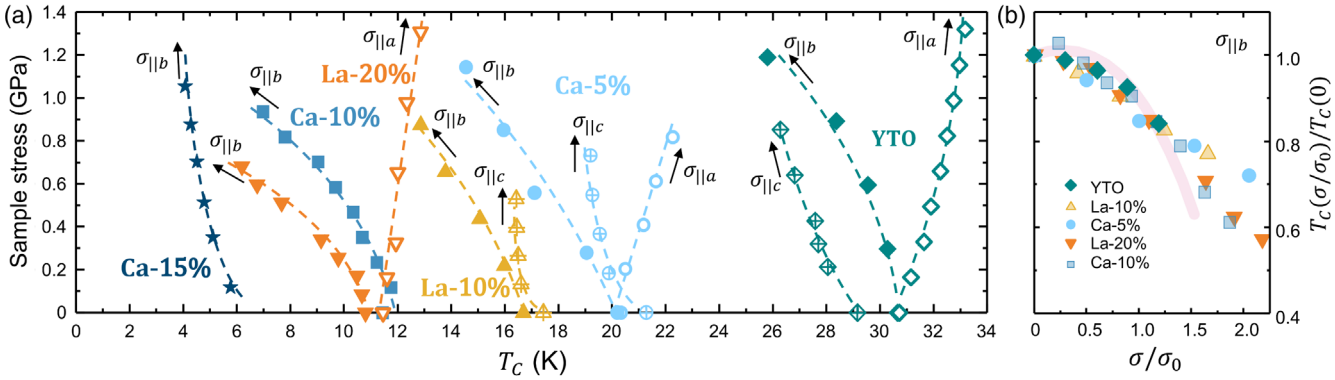

FIG. 3. (a) Phase diagram of T_C versus applied sample stress, spanning a wide range of T_C values. Empty, filled, and crossed symbols show applied stress along a, b, and c, respectively (marked as $\sigma_{||a,b,c}$). Green symbols are $YTiO_3$ (YTO). Light blue, blue, and dark blue show $Y_{0.95}Ca_{0.05}TiO_3$, $Y_{0.9}Ca_{0.1}TiO_3$, $Y_{0.85}Ca_{0.15}TiO_3$, respectively. Yellow and orange are $Y_{0.9}La_{0.1}TiO_3$ and $Y_{0.8}La_{0.2}TiO_3$, respectively. Lines are guides to the eye. Small differences between the $\sigma = 0$ transition temperatures for the same nominal compositions are due to a slight variation in oxygen offstoichiometry of crystals from the same growths [35]. (b) Single-parameter scaling of $T_C(\sigma/\sigma_0)/T_C(0)$ with stress along b. The doping-dependent scaling parameter σ_0 plays the role of an effective elastic modulus. The line shows the DFT calculation for $YTiO_3$ [same as in Fig. 4(c)]. See Ref. [25] for values of σ_0.

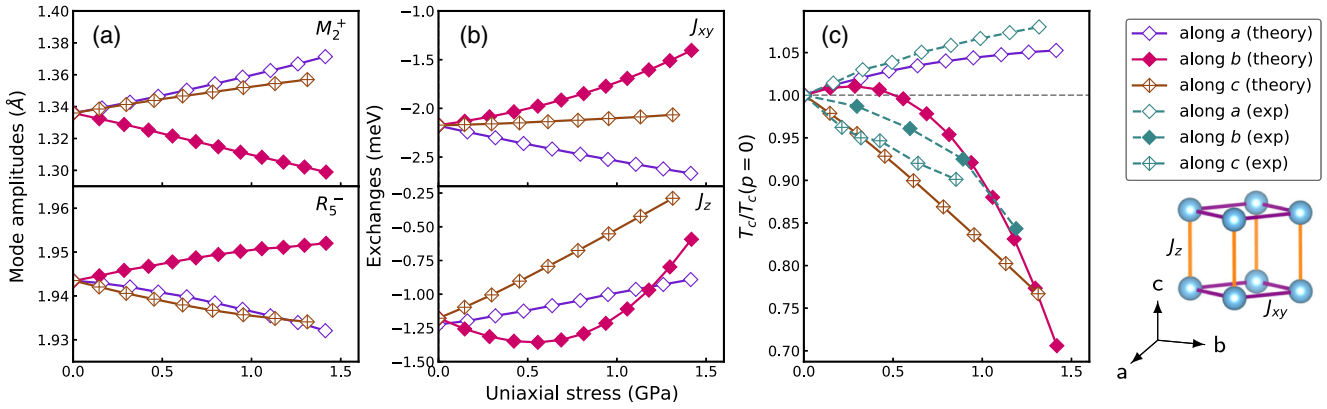

FIG. 4. DFT results for $YTiO_3$ as a function of compressive uniaxial stress along a, b, and c. (a) Mode amplitudes of the octahedral rotations corresponding to the M_2^+ and R_5^- irreps in $YTiO_3$. (b) Nearest-neighbor exchange parameters J_{xy} and J_z obtained from fits to the Heisenberg model. (c) Mean-field Curie temperatures using the DFT-obtained exchanges, including the subleading next-nearest-neighbor exchanges [25], along with experimental results for $YTiO_3$. A similar analysis for tensile strain can be found in Ref. [25].

systems were not performed due to the exceedingly high numerical cost, but given the scaling in Fig. 3(b), the results for the undoped system should also apply to doped compounds. Note that previous studies have shown the suitability of a simple nearest-neighbor Heisenberg model to capture most of the spin-wave dispersion properties [36]. Here, our main modifications are to allow for the exchange interaction to differ along in-plane and out-of-plane directions, i.e., $J_{xy} \neq J_z$ (see inset of Fig. 4) and to include subleading next-nearest-neighbor interactions [25].

We focus on the two types of octahedral rotations in $YTiO_3$, namely, the $a^0a^0c^+$ and $a^-a^-c^0$ rotation modes [Fig. 1(c)] in Glazer notation, which transform, respectively, as the irreducible representations (irreps) M_2^+ and R_5^- of the space group $Pm\bar{3}m$. We characterize the distortion magnitudes according to their irrep mode amplitudes, that may be understood as follows. Consider a general distortion of a crystal, described as a vector of atomic displacements. To determine the extent to which this distortion is composed of a particular octahedral rotation mode (corresponding to a particular irrep) we calculate the inner products of the total distortion vector with the irrep vectors. This then projects out the weight corresponding to the octahedral rotations, and the magnitude of the inner product is defined as the irrep mode amplitude. As one may expect, these mode amplitudes are proportional to the corresponding octahedral rotation modes, and for small distortions are also proportional to the rotation angles. However, angles can become ill defined for sufficiently distorted structures, while the irrep mode amplitudes are always well defined.

We find that the two types of rotations have opposite trends under uniaxial stress along different axes [Fig. 4(a)]: the M_2^+ rotation angle decreases under compressive stress along b, but increases under compressive stress along a and c. The magnitude of the R_5^- distortions has the opposite trend, as it increases under compressive stress along the b axis. Moreover, the amplitude of the R_5^- distortions is less sensitive to uniaxial stress. Given the low structural symmetry and complex multitilt system, it is not straightforward to intuitively grasp the tilt behavior with applied stress; for a more detailed analysis, see Ref. [37].

The changes in the octahedral rotations alter the Ti-O-Ti angles, which in turn significantly alters the magnetic exchange interactions [38,39], as shown in Fig. 4(b). For stress along a, both nearest-neighbor exchange interactions J_{xy} and J_z vary almost linearly with stress, with J_{xy} increasing in magnitude, whereas the magnitude of J_z decreases. We also find that J_{xy} is more sensitive to stress than J_z. This, in addition to the larger number of J_{xy} versus J_z bonds, results in an increase of mean-field T_C for stress along a, as shown in Fig. 4(c). For stress along c, J_{xy} remains mostly unchanged while J_z decreases in magnitude almost linearly, which results in a suppression of T_C with stress [Fig. 4(c)]. Finally, for uniaxial stress along b, $|J_{xy}|$ decreases while $|J_z|$ first increases with stress. These two competing behaviors lead to a slight increase in T_C for smaller stress values, as indeed also observed in experiment [Fig. 2(a)]. Yet T_C decreases rapidly under larger values of stress as $|J_z|$ also decreases. As shown in Figs. 4(c) and 3(b), in all three cases the first-principles calculations agree well with the experimentally observed relative change in T_C. This shows that the effect of stress on the magnetic properties can be explained by the crystal structural changes, and that it is mediated by the octahedral rotations.

To conclude, we have shown that the FM transition in RE titanates can be continuously tuned using uniaxial stress, and we have obtained a microscopic understanding of the underlying coupling between structural distortions, orbital overlap, and effective spin interactions. The good agreement between measured and calculated changes of T_C with

stress shows that the intricate octahedral distortions and their influence on the superexchange are well captured by our first-principles calculations. The strong and anisotropic stress response is robust across the ionic substitution phase diagram and does not rely on a nearby structural instability, which implies that these and related materials have tremendous potential for strain engineering of magnetism, including through the use of epitaxial strain and/or in heterostructures. Indeed, first-principles calculations have predicted strong effects of lattice strain on magnetism in manganese and vanadium perovskite oxides [40–42], although experimental work is still scarce and mostly focused on epitaxial strain in thin films. Additionally, in cobaltates, hydrostatic pressure seems to have a significant effect on the bandwidth and magnetic order [43,44]. Thus, uniaxial stress could be an important parameter in exploring the complex nature of magnetic transition-metal oxides. Finally, our work opens the possibility to study the (quantum) phase transitions between the FM, AFM, and paramagnetic ground states using homogeneous uniaxial stress as a control variable. The spin-lattice coupling for deformation along b is large enough to induce such a transition in the $Y_{0.85}Ca_{0.15}TiO_3$ sample studied here, but our result indicates that the transition may not be continuous. A first-order transition and associated phase separation regime could be a generic feature of this hole-doped system, which recent experiments have shown the metal-insulator transition to involve phase separation [23], yet more work is needed to clarify this issue, in particular uniaxial stress experiments on nominally stoichiometric materials that are closer to the phase boundaries than $YTiO_3$. In this regard, we note that it was recently proposed that uniaxial strain in isovalent chemically substituted RE titanates could be used to induce a quantum critical end-point [45].

We thank M. Lukas and C. Leighton for fruitful comments and discussions. The work at the University of Minnesota was funded by the Department of Energy through the University of Minnesota Center for Quantum Materials, under Grant No. DE-SC-0016371. The work at the University of Zagreb was supported by the Croatian Science Foundation through Grant No. IP-01-2018-2970.

[1] J. H. Haeni, P. Irvin, W. Chang, R. Uecker, P. Reiche, Y. L. Li, S. Choudhury, W. Tian, M. E. Hawley, B. Craigo, A. K. Tagantsev, X. Q. Pan, S. K. Streiffer, L. Q. Chen, S. W. Kirchoefer, J. Levy, and D. G. Schlom, Nature (London) **430**, 758 (2004).

[2] N. Takeshita, T. Sasagawa, T. Sugioka, Y. Tokura, and H. Takagi, J. Phys. Soc. Jpn. **73**, 1123 (2004).

[3] F. Hardy, N. J. Hillier, C. Meingast, D. Colson, Y. Li, N. Barišić, G. Yu, X. Zhao, M. Greven, and J. S. Schilling, Phys. Rev. Lett. **105**, 167002 (2010).

[4] J.-H. Chu, J. G. Analytis, K. De Greeve, P. L. McMahon, Z. Islam, Y. Yamamoto, and I. R. Fisher, Science **329**, 824 (2010).

[5] C. W. Hicks, D. O. Brodsky, E. A. Yelland, A. S. Gibbs, J. A. Bruin, M. E. Barber, S. D. Edkins, K. Nishimura, S. Yonezawa, Y. Maeno, and A. P. Mackenzie, Science **344**, 283 (2014).

[6] A. Steppke, L. Zhao, M. E. Barber, T. Scaffidi, F. Jerzembeck, H. Rosner, A. S. Gibbs, Y. Maeno, S. H. Simon, A. P. Mackenzie, and C. W. Hicks, Science **355**, eaaf9398 (2017).

[7] V. Grinenko, S. Ghosh, R. Sarkar, J.-C. Orain, A. Nikitin, M. Elender, D. Das, Z. Guguchia, F. Brückner, M. E. Barber, J. Park, N. Kikugawa, D. A. Sokolov, J. S. Bobowski, T. Miyoshi, Y. Maeno, A. P. Mackenzie, H. Luetkens, C. W. Hicks, and H. H. Klauss, Nat. Phys. **17**, 748 (2021).

[8] Z. Shao, X. Cao, H. Luo, and P. Jin, NPG Asia Mater. **10**, 581 (2018).

[9] N. B. Aetukuri, A. X. Gray, M. Drouard, M. Cossale, L. Gao, A. H. Reid, R. Kukreja, H. Ohldag, C. A. Jenkins, E. Arenholz, K. P. Roche, H. A. Dürr, M. G. Samant, and S. S. P. Parkin, Nat. Phys. **9**, 661 (2013).

[10] H.-H. Kim, S. M. Souliou, M. E. Barber, E. Lefrançois, M. Minola, M. Tortora, R. Heid, N. Nandi, R. A. Borzi, G. Garbarino, A. Bosak, J. Porras, T. Loew, M. König, P. J. W. Moll, A. P. Mackenzie, B. Keimer, C. W. Hicks, and M. Le Tacon, Science **362**, 1040 (2018).

[11] C. Dhital, Z. Yamani, W. Tian, J. Zeretsky, A. S. Sefat, Z. Wang, R. J. Birgeneau, and S. D. Wilson, Phys. Rev. Lett. **108**, 087001 (2012).

[12] Z. Guguchia, D. Das, C. N. Wang, T. Adachi, N. Kitajima, M. Elender, F. Brückner, S. Ghosh, V. Grinenko, T. Shiroka, M. Müller, C. Mudry, C. Baines, M. Bartkowiak, Y. Koike, A. Amato, J. M. Tranquada, H.-H. Klauss, C. W. Hicks, and H. Luetkens, Phys. Rev. Lett. **125**, 097005 (2020).

[13] M. Mochizuki and M. Imada, New J. Phys. **6**, 154 (2004).

[14] D. A. MacLean, H.-N. Ng, and J. E. Greedan, J. Solid State Chem. **30**, 35 (1979).

[15] W. Knafo, C. Meingast, A. V. Boris, P. Popovich, N. N. Kovaleva, P. Yordanov, A. Maljuk, R. K. Kremer, H. v. Löhneysen, and B. Keimer, Phys. Rev. B **79**, 054431 (2009).

[16] J. Hemberger, H.-A. Krug von Nidda, V. Fritsch, J. Deisenhofer, S. Lobina, T. Rudolf, P. Lunkenheimer, F. Lichtenberg, A. Loidl, D. Bruns, and B. Büchner, Phys. Rev. Lett. **91**, 066403 (2003).

[17] A. C. Komarek, H. Roth, M. Cwik, W.-D. Stein, J. Baier, M. Kriener, F. Bourée, T. Lorenz, and M. Braden, Phys. Rev. B **75**, 224402 (2007).

[18] J. E. Greedan, J. Less-Common Met. **111**, 335 (1985).

[19] T. Katsufuji, Y. Taguchi, and Y. Tokura, Phys. Rev. B **56**, 10145 (1997).

[20] Y. Okimoto, T. Katsufuji, Y. Okada, T. Arima, and Y. Tokura, Phys. Rev. B **51**, 9581 (1995).

[21] J. P. Goral, J. E. Greedan, and D. A. MacLean, J. Solid State Chem. **43**, 244 (1982).

[22] Y. Tokura, Physica (Amsterdam) **237-238B**, 1 (1997).

[23] S. Hameed, J. Joe, D. M. Gautreau, J. W. Freeland, T. Birol, and M. Greven, Phys. Rev. B **104**, 045112 (2021).

[24] Z. Y. Zhao, O. Khosravani, M. Lee, L. Balicas, X. F. Sun, J. G. Cheng, J. Brooks, H. D. Zhou, and E. S. Choi, Phys. Rev. B **91**, 161106(R) (2015).

[25] See Supplemental Material at http://link.aps.org/supplemental/10.1103/PhysRevLett.128.167201 for details on the experimental setup and the first-principles calculations, which includes Refs. [26–31].
[26] G. Kresse and J. Hafner, Phys. Rev. B **47**, 558 (1993).
[27] G. Kresse and J. Furthmüller, Comput. Mater. Sci. **6**, 15 (1996).
[28] G. Kresse and J. Furthmüller, Phys. Rev. B **54**, 11169 (1996).
[29] J. P. Perdew, A. Ruzsinszky, G. I. Csonka, O. A. Vydrov, G. E. Scuseria, L. A. Constantin, X. Zhou, and K. Burke, Phys. Rev. Lett. **100**, 136406 (2008).
[30] S. L. Dudarev, G. A. Botton, S. Y. Savrasov, C. J. Humphreys, and A. P. Sutton, Phys. Rev. B **57**, 1505 (1998).
[31] B. J. Campbell, H. T. Stokes, D. E. Tanner, and D. M. Hatch, J. Appl. Crystallogr. **39**, 607 (2006).
[32] D. Pelc, Z. W. Anderson, B. Yu, C. Leighton, and M. Greven, Nat. Commun. **10**, 2729 (2019).
[33] S. Hameed, D. Pelc, Z. W. Anderson, A. Klein, R. J. Spieker, L. Yue, B. Das, J. Ramberger, M. Lukas, Y. Liu, M. J. Krogstad, R. Osborn, Y. Li, C. Leighton, R. M. Fernandes, and M. Greven, Nat. Mater. **21**, 54 (2022).
[34] S. Hameed *et al.*, Phys. Rev. B **104**, 024410 (2021).
[35] S. Hameed, J. Joe, L. R. Thoutam, J. Garcia-Barriocanal, B. Yu, G. Yu, S. Chi, T. Hong, T. J. Williams, J. W. Freeland, P. M. Gehring, Z. Xu, M. Matsuda, B. Jalan, and M. Greven, Phys. Rev. Mater. **5**, 125003 (2021).
[36] C. Ulrich, G. Khaliullin, S. Okamoto, M. Reehuis, A. Ivanov, H. He, Y. Taguchi, Y. Tokura, and B. Keimer, Phys. Rev. Lett. **89**, 167202 (2002).
[37] D. Gautreau, Z. Wang, R. M. Fernandes, and T. Birol (to be published).
[38] J. Goodenough, *Magnetism and the Chemical Bond*, Interscience Monographs on Chemistry (R.E. Krieger Publishing Company, Huntington, 1976).
[39] T. Birol, N. A. Benedek, H. Das, A. L. Wysocki, A. T. Mulder, B. M. Abbett, E. H. Smith, S. Ghosh, and C. J. Fennie, Curr. Opin. Solid State Mater. Sci. **16**, 227 (2012).
[40] P. Rivero, V. Meunier, and W. Shelton, Phys. Rev. B **93**, 094409 (2016).
[41] R. Qiu, E. Bousquet, and A. Cano, J. Phys. Condens. Matter **29**, 305801 (2017).
[42] P. Horsch, A. M. Oleś, L. F. Feiner, and G. Khaliullin, Phys. Rev. Lett. **100**, 167205 (2008).
[43] I. Fita, R. Szymczak, R. Puzniak, I. O. Troyanchuk, J. Fink-Finowicki, Y. M. Mukovskii, V. N. Varyukhin, and H. Szymczak, Phys. Rev. B **71**, 214404 (2005).
[44] K. Mydeen, P. Mandal, D. Prabhakaran, and C. Q. Jin, Phys. Rev. B **80**, 014421 (2009).
[45] Z. Wang, D. Gautreau, T. Birol, and R. M. Fernandes, Phys. Rev. B **105**, 144404 (2022).